CrossMark

Biosynthesis of SnO$_2$ nanoparticles by aqueous leaf extract of *Calotropis gigantea* for photocatalytic applications

T. T. Bhosale[1,2] · H. M. Shinde[1,2] · N. L. Gavade[1] · S. B. Babar[1] · V. V. Gawade[1] · S. R. Sabale[3] · R. J. Kamble[3] ·
B. S. Shirke[2] · K. M. Garadkar[1]

Abstract
Here we developed biogenic route for the synthesis of SnO$_2$ NPs by using aqueous leaf extract of *Calotropis gigantea* which acts as reducing and stabilizing agent. The biosynthesized SnO$_2$ NPs were characterized by different characterization techniques such as UV–visible diffuse reflectance spectroscopy (DRS), X-ray diffraction (XRD), Fourier transform infrared spectroscopy (FT-IR), field emission scanning electron microscopy (FE-SEM), energy dispersive X-ray analysis and high resolution transmission electron microscope. XRD pattern shows tetragonal structure of SnO$_2$ NPs with 35 nm size. The FT-IR spectra of aqueous leaf extract shows the presence of hydroxyl group, aldehydes, amines and aromatic rings which are responsible for biochemical transformation. The FE-SEM analysis suggests mixed morphology with slight agglomeration. DRS absorption spectrum indicates the band gap is about 3.1 eV. The photocatalytic activity of the synthesized SnO$_2$ NPs checked for the degradation of Methyl Orange and found up to 80% degradation within 3 h under UV–visible light.

1 Introduction

Nanotechnology is an advanced technology which deals with the preparation, processing and applications of nanomaterials. Nanoscale metal oxide semiconductors have been the subject of extensive research due to their unique properties [1]. In the world of Nanotechnology, Nanomaterials are of great interest due to their small size and amazing properties like large surface area, modified and easily tuneable morphology [2, 3]. Industries like paper, plastic, textile and rubber widely use the dyes which lead to severe environmental contamination due to the emission of the coloured and toxic wastewater into water bodies [4]. Hence to the removal of organic compounds from water and to decrease the concentration of organic dyes, the use of photocatalyst is considered as most encouraging way [5]. In recent years the novel heterogeneous metal oxide semiconductor materials have been developed and attracted considerable attention owing to their photocatalytic ability in the degradation of various environmental pollutants such as detergents, pesticides, dyes and volatile organic compounds under UV light irradiation to substitute the traditional waste water treatment [6].

SnO$_2$ is one of the most intriguing materials today, since it is a well-known n-type semiconductor with a wide band gap of 3.6 eV, therefore it is used in transparent conductive electrode for solar cells, gas sensors, photoconductive and photochemical device in liquid crystal display and lithium ion batteries [7]. SnO$_2$ nanoparticles (NPs) are also suitable to use as a photocatalyst because of high surface to volume ratio which results in increased sensitivity and adsorption [8, 9].

There are many reports on the synthesis of SnO$_2$ NPs by conventional methods like spray pyrolysis, hydrothermal, chemical vapour deposition and sol–gel [10–13] but physical methods are highly expensive, while the chemical methods are harmful to the environment and living organisms [14–16]. Due to negative impact of chemical methods to the environment there is urgent need to replace chemical methods by environment friendly methods. The use of plants for the synthesis of NPs could be advantageous due to environmentally benign biological process as this eliminates the

✉ K. M. Garadkar
kmg_chem@unishivaji.ac.in

1   Nanomaterials Research Laboratory, Department
    of Chemistry, Shivaji University, Kolhapur,
    Maharashtra 416004, India

2   Material Science Laboratory, Department of Chemistry,
    Y. C. Warana Mahavidyalaya, Warananagar,
    Maharashtra 416113, India

3   P.G. Department of Chemistry, Jaysingpur College,
    Jaysingpur, Maharashtra 416 101, India

elaborative process of maintaining cell culture [17]. Also, synthesis of nanomaterials using plant extract is the simplest approach because of its low-cost and ease operation [18]. A new branch of nanotechnology is called nanobiotechnology which combines biological principles with physical and chemical procedures to generate nanosized particles with specific function [19].

The leaf extract of *Calotropis gigantea* (C. G.) is used for are the synthesis of AgNPs [20], CuO [21] and ZnO [22]. Even though there are various methods available for the synthesis of SnO_2, the biosynthesis of SnO_2 was only reported by using *Erwiniaherbicola* [23].

In the present study, the green synthesis of SnO_2 NPs achieved by using aqueous leaf extract of C. G. leaves. There are two species of Calotropis viz. C. G. and *Calotropis procera* having great similarity in the chemical properties. Many phytochemical constituents in various parts of Calotropis mainly in the leaves, the constituents like Uscharin, gigantin, calcium oxalate, α and β calotropeol, β amyrin, saturated and unsaturated fatty acids, hydrocarbons, acetates and benzoates, flavonoids, triterpenoids, steroids, triterpenoids, saponins, terpenes, alcohols, resins and esters of calotropeols, volatile long chain fatty acids, glycosides and proteases have been found in various parts of Calotropis. The milky latex of plant is rich in lupeol, calotropin, calotoxin and Uscharidin, the latex protein [24].

2 Materials and methods

Tin (IV) chloride pentahydrate ($SnCl_4 \cdot 5H_2O$) was purchased from Fume chemicals, India Pvt Ltd. The C. G. leaves were collected from Kolhapur district (India). All the chemicals were of analytical grade and used as received. The solutions were prepared in Millipore water obtained from Millipore water system (Millipore Corp., Bangalore, India). All the glassware used were properly washed with distilled water and dried in hot air oven.

2.1 Preparation of leaf extract of C. G.

For the preparation of leaf extract of C. G., the fresh leaves were washed many times with distilled water and dried under sunlight. Then 4 g of dried leaves were crushed, boiled in 100 mL distilled water for 15 min until the formation of yellow colour solution. The solution was kept to attain room temperature; then the leaf extract was filtered through Whatmann filter paper No.1 and stored in the refrigerator.

2.2 Synthesis of SnO_2 NPs

For the synthesis of SnO_2 NPs, 10 mL of C. G. leaf extract was diluted to 100 mL with distilled water and added dropwise into the 40 mL of $SnCl_4 \cdot 5H_2O$ (0.05 M) solution with constant stirring. After complete addition of leaf extract, a gelatinous precipitate was obtained. Then the precipitate was washed several times using distilled water and dried in the microwave oven at 900 W for 20 min (20 s on 40 s off cycle). The obtained dried powder was then grounded by using mortar and pestle. Further the calcinations of powder were carried at 400 °C for 3 h. The schematic representation of formation of SnO_2 NPs is shown in Fig. 1. The synthesized powder further mashed in the mortar and pestle for the further characterization.

2.3 Qualitative phytochemical screening of C. G. leaf extract

The C G. leaf extract was subjected to chemical tests for the identification of their active constituents. The chemical tests were performed by reported methods [25, 26].

2.3.1 Test for tannins

1 g of C. G. dried leaf powder was boiled in 40 mL distilled water. In the filtrate, $FeCl_3$ (0.1%) was added which gives brownish green colour to the mixture, shows presence of tannin in the plant extract [25].

2.3.2 Test for saponins

5 mL of distilled water was added to 10 mL of leaf extract, and the mixture is vigorously stirred for few minutes, when few drops of olive oil added in this mixture and stirred, it forms froath. This shows the presence of saponins [25].
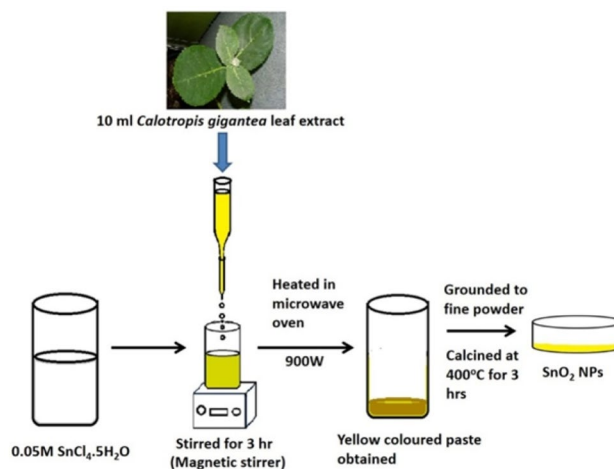

Fig. 1 Schematic representation for the synthesis of SnO_2 NPs

2.3.3 Test for flavonoids

To the aqueous leaf extract, 10 mL of ethyl acetate was added and the test tube containing this mixture was heated in the water bath. 1 mL of dilute ammonia was added to this mixture, which gives yellow colour, i.e., presence of flavonoids [25].

2.3.4 Test for terpenoid

Leaf extract was taken in a test tube and 2 mL of ammonia was added. The test tube was kept in water bath to cool and 3 mL of conc. H_2SO_4 was added from the side of the test tube. This shows reddish brown colour at the interface indicates the presence of terpenoids [25].

2.3.5 Test for steroids

2 mL conc. H_2SO_4 was added to the 1 mL ethanolic extract, and then 2 mL of acetic anhydride was added. There is no change in the colour of extract from Violet to Blue or Green. This indicates steroids are absent [25].

2.3.6 Test for phenols

5% ferric chloride was added to the 2 mL leaf extract which shows black colouration. This indicates presence of phenols [26].

2.3.7 Test for alkaloids (Mayer's test)

Mayer's test reagent was added to 2 mL of leaf extract which gives cream coloured precipitation. i.e., presence of alkaloids [26].

2.3.8 Test for proteins (Biuret test)

The leaf extract was heated with distilled water and filtered. To this filtrate 2% $CuSO_4$, 95% ethanol and KOH was added which form a pink ethanolic layer. This indicate the presence of proteins [26].

2.3.9 Test for quinons

5 mL of leaf extract was treated with 2 mL of concentrated HCl, this shows yellow precipitation. This indicates the presence of quinons [26].

From Table 1, we observed that the plant of C. G. contains higher amount of flavonoids and phenols that are important for complex formation with tin (Sn^{4+}). Other

Table 1 Phytochemical constituent present in aqueous leaf extract of *Calotropis gigantea*

S. no.	Constituents	Results
1	Alkaloids	+
2	Tannins	+
3	Saponins	+
4	Flavonoids	++
5	Terpenoids	+
6	Steroids	–
7	Phenols	++
8	Proteins	+
9	Quinons	+

constituents like alkaloids, terpenoids, etc. also present. The content of Steroids are absent in the plant.

2.4 Characterization

The prepared SnO_2 NPs were characterized thoroughly by using different characterization techniques. The powder X-ray diffraction (XRD) patterns of catalyst were recorded by using Bruker Analytical Instrument, Germany [Model-D2 PHASER (Cu Kα)]. Diffuse reflectance spectrums (DRS) of SnO_2 NPs were obtained using UV–Vis (JASCO V-770 spectrophotometer). FT-IR spectra were obtained using a FT-IR (JASCO-4600). TEM images were scanned with JEOL-JEM 2100 equipped with high-resolution Gatan CCD camera. The SEM-EDS images were obtained using (JEOL-JSM-6360).

2.5 Photocatalytic degradation of Methyl Orange

Photocatalytic activity of the synthesized SnO_2 NPs was tested for the degradation of Methyl Orange (MO) as a model pollutant under UV-light. High-pressure mercury lamp (250 W) was used as a UV light source. The photocatalytic experiment was carried out in photoreactor which was kept open in the air for photo-oxidation reaction. The optimum quantity of SnO_2 was obtained by varying the amount of SnO_2 from 0.5 to 2.0 mg in 100 mL of MO solution (20 ppm). Prior to irradiating the solution with UV light, 150 mg of catalyst was suspended into 100 mL of MO solution at neutral pH and magnetically stirred for 30 min in dark to ensure adsorption–desorption equilibrium. After irradiating the solution with UV-light, at periodic time intervals 0 to 30 min, 3 mL reaction mixture was withdrawn, centrifuged, and the supernatant solution was collected and optical density (OD) measured by using UV–visible spectrophotometer.
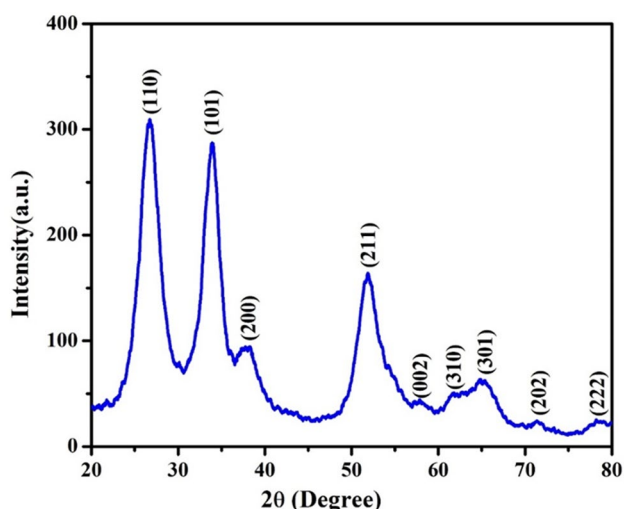
Fig. 2 XRD pattern of SnO$_2$ NPs

3 Results and discussion

3.1 X-ray diffraction

The XRD pattern of the synthesized SnO$_2$ NPs is shown in Fig. 2. The peaks at 2θ values of 26.5°, 34°, 37.9°, 51.7°, 54.4°, 57.7°, 61.7°, 64.8°, 71.3° and 78.5° associated with (110), (101), (200), (211), (220), (002), (310), (301), (202) and (222) planes respectively that indicates the formation of SnO$_2$ with tetragonal structure according to JCPDS card no. 77-0452. The average crystallite size of SnO$_2$ NPs was found to be 35 nm calculated from Scherrer's equation.

$$D = k\lambda / \beta \cos\theta$$

where λ is the X-ray wavelength of Cu Kα (1.54 Å), θ is the Bragg's angle, β is the full width at the half maximum in radians and k is unknown shape factor.

3.2 FE-SEM and EDS analysis of SnO$_2$ NPs

The morphology of biosynthesized SnO$_2$ NPs was observed by using FE-SEM. Figure 3 shows FE-SEM images with different magnification. This shows agglomeration of poly dispersed nanostructures of SnO$_2$. The agglomeration effect depends on the size of the particles. According to XRD analysis, the estimated average crystallite size is found to be 35 nm, as the particle size move towards the nanoscale, the agglomeration gets increased [27].

Figure 4 shows EDS spectrum of biosynthesized SnO$_2$ NPs, which represents intense peaks of Sn and O at 3.6, 0.5 eV respectively. The presence of intense peaks of both Sn and O clearly indicates the composition is pure SnO$_2$. Few weak signals of copper (Cu), phosphorous (P), nitrogen (N) and carbon (C) are also recognized due to the presence of biomolecules like aldehydes, amines, terpenoids and phenolic compounds in plant extract. The Cu and C signals may be associated with grid used for SEM analysis.

3.3 TEM images of SnO$_2$ NPs

TEM analysis was taken to obtain the information about the size and morphology of the SnO$_2$ NPs. Figure 5a, b shows TEM images of SnO$_2$ NPs with various magnifications. It can be rightly seen that the formed SnO$_2$ NPs are irregularly agglomerated and the average size is about 30–40 nm. The d spacing of 0.33 nm is observed which is well agree with the values of d which are obtained from XRD proves the tetragonal structure of SnO$_2$ and shown in Fig. 5c. Figure 5d
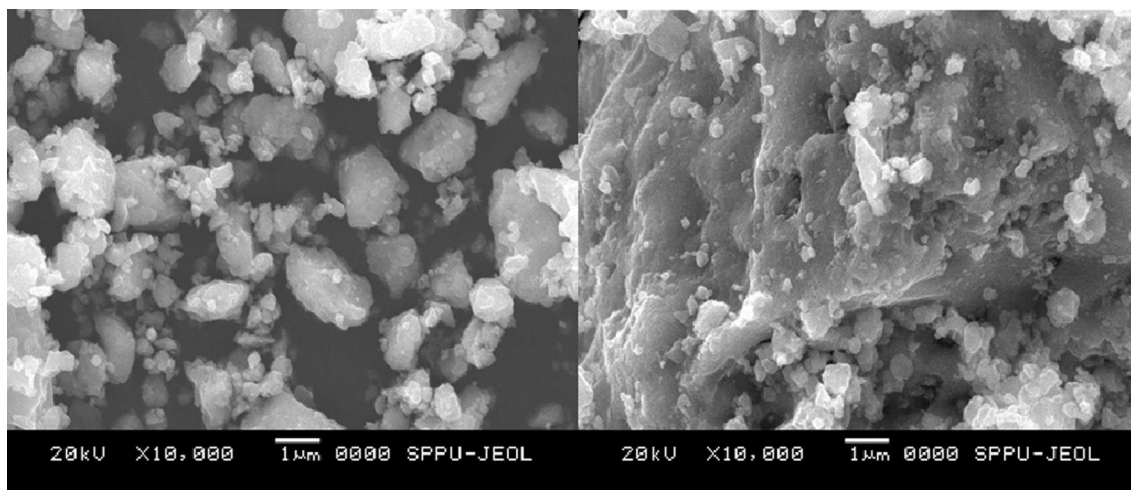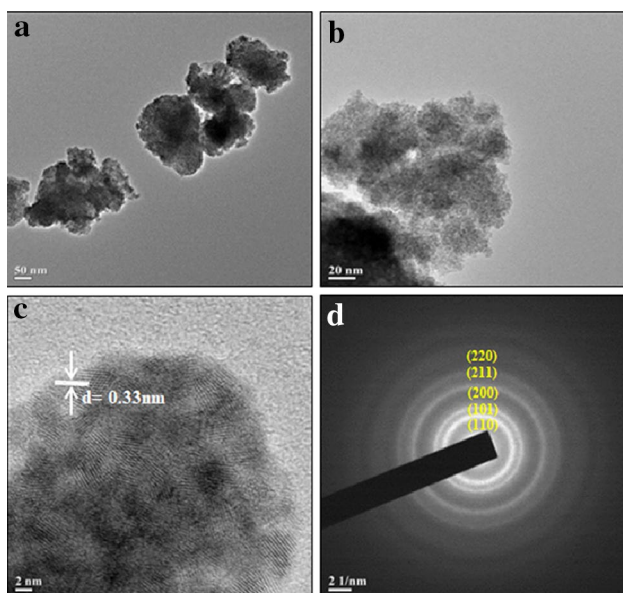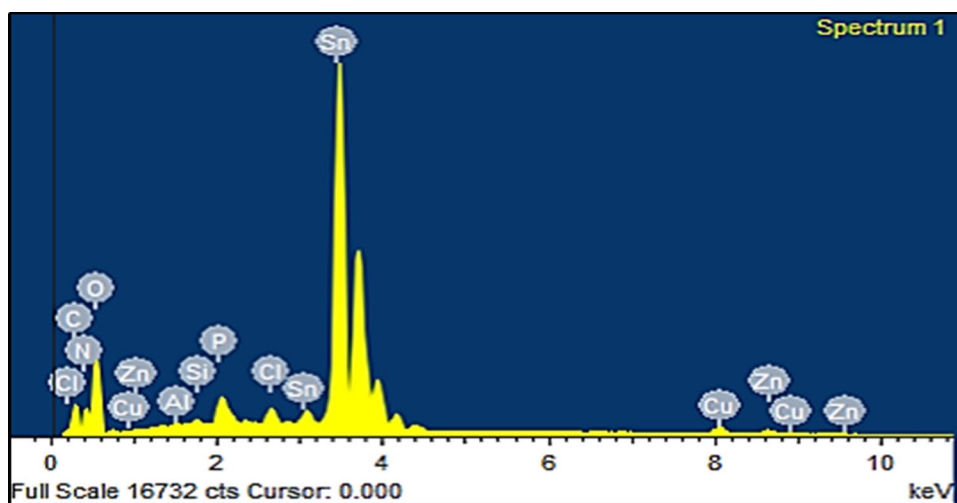

Fig. 3 SEM images of biosynthesized SnO$_2$ NPs

Fig. 4 EDS Image of SnO$_2$ NPs

Fig. 5 **a, b** TEM images of SnO$_2$ NPs with different magnifications, **c** HR-TEM of SnO$_2$ and **d** SAED pattern of SnO$_2$

shows the selected area electron diffraction pattern (SAED) of SnO$_2$ NPs. From SAED pattern, it is indicates that the particles are nanocrystalline in nature.

3.4 UV–Vis diffuse reflectance spectrum of SnO$_2$ NPs

Figure 6 shows UV–Vis DRS of SnO$_2$ NPs. It can be seen that the material has good absorption capacity in the visible region in the range of 400–700 nm. The plot of $(\alpha h\nu)^2$ versus photon energy (hν) was obtained to determine accurate band gap of SnO$_2$ NPs (Fig. 7). The band gap was found to be 3.1 eV, which suggest that the biogenically synthesized material is useful for photocatalytic applications.
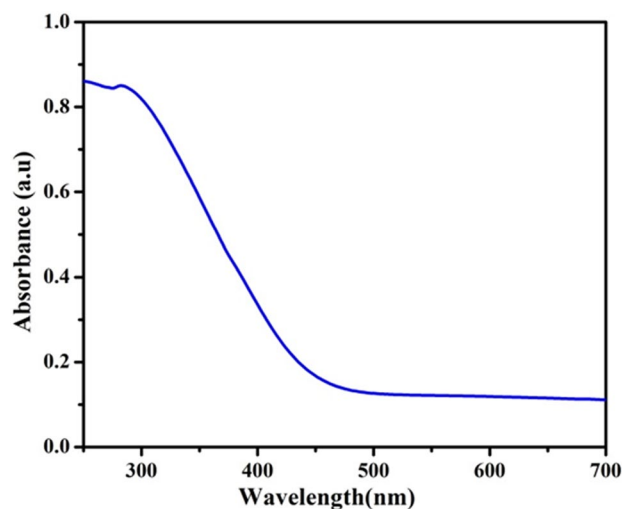
Fig. 6 UV–Vis DRS of SnO$_2$ NPs

3.5 FT-IR analysis of SnO$_2$ nanoparticles

Figure 8a shows FT-IR spectra of leaf extract. The broad and intense band at 3237–3465 cm^{-1} shows O–H stretching [28]. The absorption at 1632 cm^{-1} owing an aromatic ring [29]. The bands located at 1040 and 650 cm^{-1} represents the C–N and N–H stretching vibrations of amines, respectively [30, 31]. Broad bands at 3287, 1632, 2106 cm^{-1} shows the presence of hydroxyl group, aldehydes, amines and aromatic ring. Figure 8b shows FT-IR spectrum of SnO$_2$ NPs. The band appearing at 3480 cm^{-1} is corresponds to O–H stretching vibrations due to absorbed water on the sample surface [32]. The presence of an intense band positioned between 562 and 655 cm^{-1} related to the Sn–O–Sn vibrations which confirms the presence of SnO$_2$ as a crystalline structure [31].
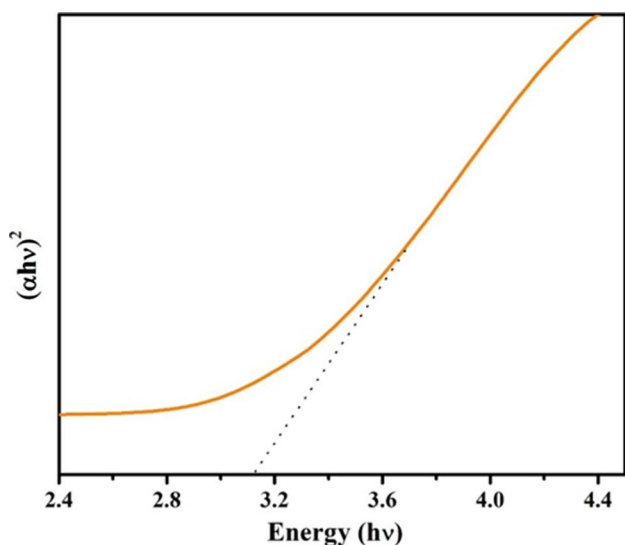
Fig. 7 A plot of $(\alpha h\nu)^2$ versus photon energy $(h\nu)$

3.6 Plausible reaction mechanism of SnO₂ NPs

The probable reaction mechanism of formation of SnO_2 NPs is shown in Fig. 9. When $SnCl_4.5H_2O$ salt solution is mixed with C. G. leaf extract, the Sn^{4+} ions distribute steadily in the solution and form a complex with active sites of hydroxyl groups. The formed complex decomposes when subjected to calcination. Polyphenolic molecules that interact with tetravalent Sn^{4+} cation forming bridge like network between two OH groups from two different chains of polyphenolic group. The tetravalent Sn^{4+} cations keeps the polyphenolic molecules together [20].

3.7 Photocatalytic properties

Figure 10 shows the degradation of MO dye under UV light by using SnO_2 photocatalyst. The concentration of MO dye decreases gradually under UV light after the addition of SnO_2. When the solution mixture was irradiated for 210 min, the degradation of MO (20 ppm) found to be 78%.

3.7.1 Effect of catalyst loading

The effect of catalyst loading on the degradation of MO dye was determined by varying the amount of catalyst as 50, 100, 150 and 200 mg that shows 2.58, 15, 32 and 19.35% of MO (20 ppm) degradation respectively in 60 min. High degradation rate was observed with 150 mg of the catalyst. The effect of loading different amount of catalyst SnO_2 on the degradation of MO dye is depicted in Fig. 11.

From Fig. 11 it is clear that as catalyst loading increases from 50 to 150 mg the rate of degradation of MO dye increases thereafter the degradation rate decreases, the maximum decolourization occurred at 150 mg of SnO_2. As the catalyst dosage increases, the total active surface area increases due to which more active sites on catalyst surface are available [33]. Below optimal amount, the number of catalytic active sites is less due to which there is decrease in the production of reactive species takes place resulting in low percentage degradation. Above the optimal catalyst amount, particle–particle interaction increases hence the solution becomes turbid which affects the poor light absorption and loss of charge carriers before surface reaction resulting in low percentage degradation. The optimum catalyst loading is found to be dependent on the initial concentration of MO solution [34].
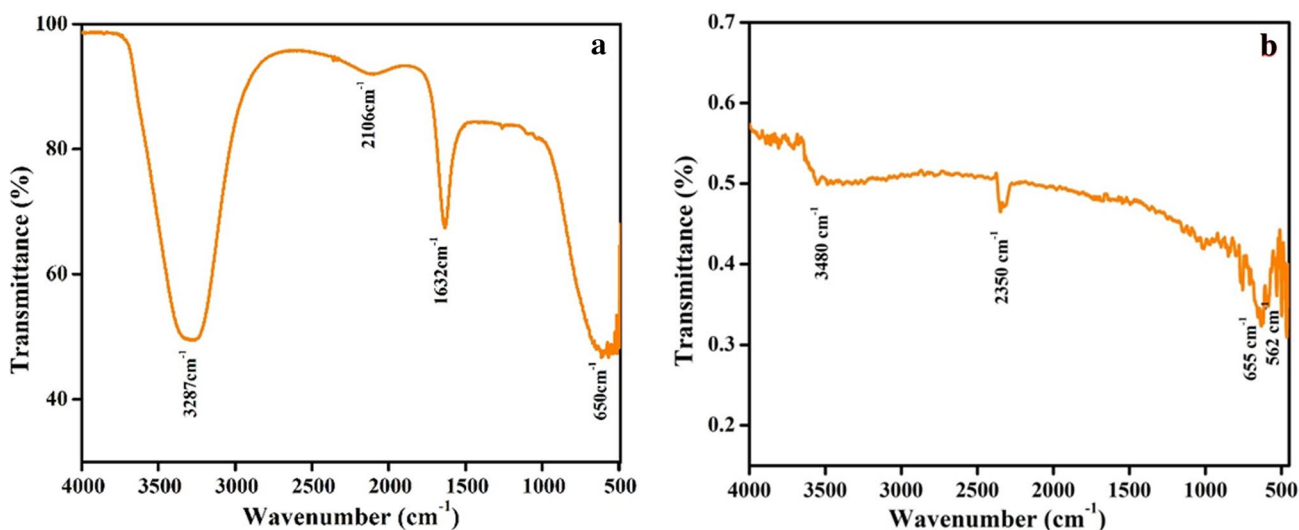

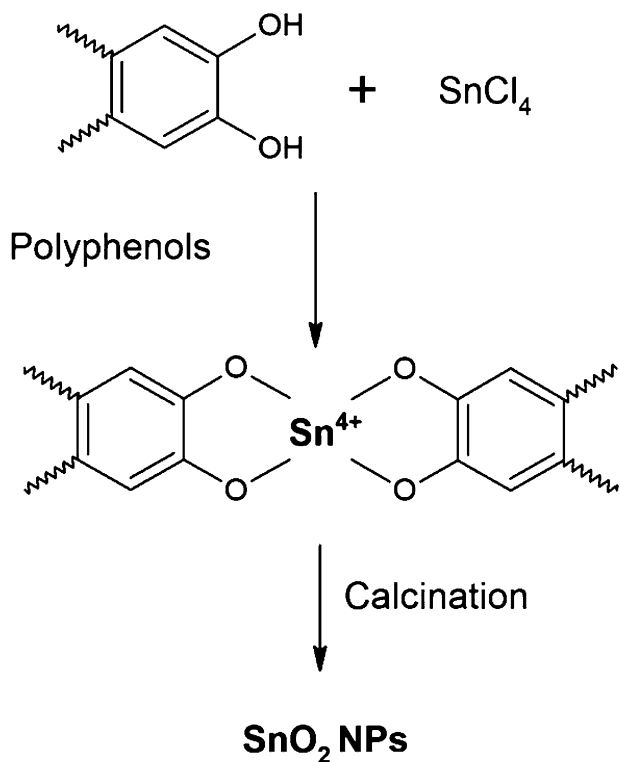**Fig. 8** **a** FT-IR spectrum of *Calotropis gigantea* leaf extract, **b** FT-IR spectrum of SnO₂ NPs

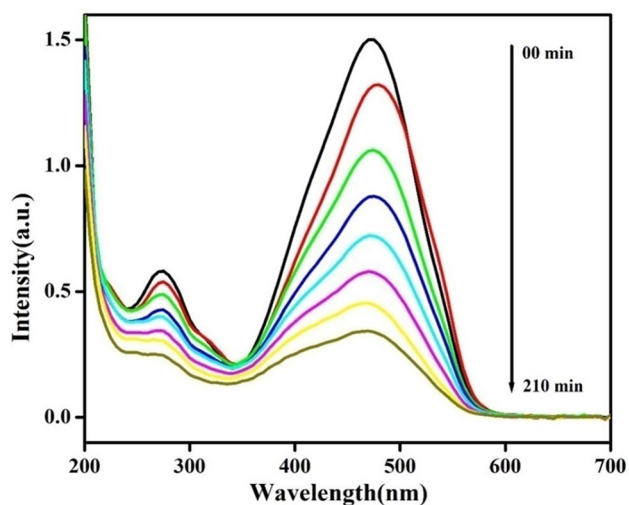Fig. 9 Plausible mechanism for the formation of SnO$_2$ NPs

Fig. 11 Effect of amount of catalyst on degradation of MO

Fig. 10 Photocatalytic degradation of MO dye under UV light
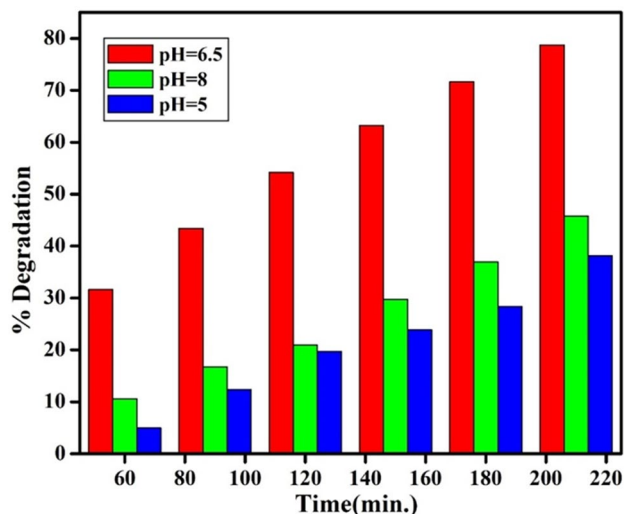
Fig. 12 Effect of pH on MO dye degradation

3.7.2 Effect of pH

Figure 12 shows the effect of pH of MO dye on the degradation rate when the catalyst amount taken is 150 mg. The results show that photodegradation of MO is highest at pH 6.5 while in both acidic and alkaline medium the degradation rate is low. It can be attributed to the surface
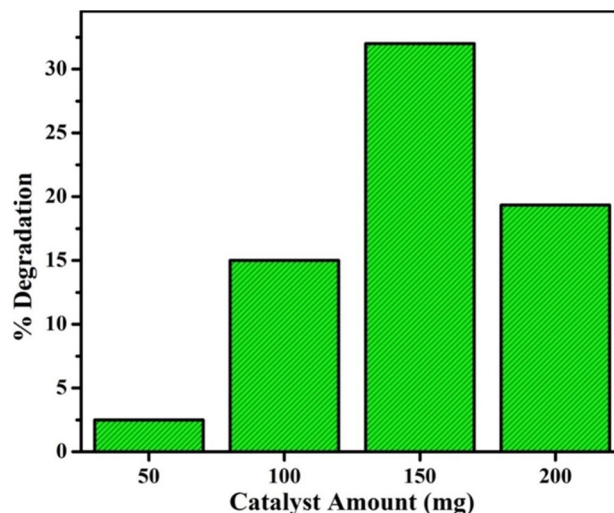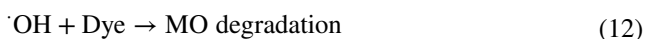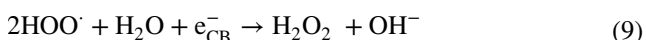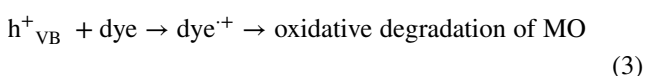
charge of nanoparticles. Whereas, the acidity of suspensions can be affected on the surface charge and dispersion of nanoparticles. Therefore, the dispersion of nanoparticles in the suspension enhance with respect to the surface charge of nanoparticles [35]. The % degradation is higher in acidic condition, because the organic compound in the solution react with the dissolved oxygen into ground state charge transfer compound, which become into inspiring state under light and dissociating into R and O unrestricted radicals in the acidic condition, this accelerate the photo oxidation of organic compound. At pH 6.5 there is no surface charge on SnO$_2$ due to Van Der Waal's forces this benefits the disperse. Hence at pH 6.5, the degradation efficiency of SnO$_2$ is higher [36].

3.7.3 Mechanism of photodegradation

When the catalyst surface is illuminated with the light energy higher than its band gap energy, it leads to the formation of holes (h^+) in the valence band and an electron (e^-) in the conduction band of SnO_2 NPs (Eq. 1).

The holes (h^+) act as an oxidizing agent and oxidize the pollutant directly or react with water to form hydroxyl radicals (Eq. 5) while the electrons (e^-) in the conduction band acts as a reducing agent and reduce the oxygen adsorbed on the surface of SnO_2 (Eq. 6). The probable mechanism for the photodegradation of MO is shown below [34].

$$SnO_2 + h \rightarrow SnO_2 + e^-_{CB} + h^+_{VB} \tag{1}$$

$$e^-_{CB} + h^+_{VB} \rightarrow heat \ (unproductive) \tag{2}$$

$$h^+_{VB} + dye \rightarrow dye^{\cdot+} \rightarrow oxidative \ degradation \ of \ MO \tag{3}$$

$$h^+_{VB} + H_2O \rightarrow H^+ + OH^{\cdot} \tag{4}$$

$$h^+_{VB} + HO^- \rightarrow OH^{\cdot} \tag{5}$$

$$O_2 + e^-_{CB} \rightarrow O_2^{\cdot-} \tag{6}$$

$$O_2^{\cdot-} + 2H_2O \rightarrow HOO^{\cdot} + 2HO \tag{7}$$

$$2HOO^{\cdot} + H_2O + e^-_{CB} \rightarrow HOO^{\cdot-} + 2HO \tag{8}$$

$$2HOO^{\cdot} + H_2O + e^-_{CB} \rightarrow H_2O_2 + OH^- \tag{9}$$

$$H_2O_2 + e^-_{CB} \rightarrow {}^{\cdot}OH + OH \tag{10}$$

$$H_2O_2 + h \rightarrow 2^{\cdot}OH \tag{11}$$

$${}^{\cdot}OH + Dye \rightarrow MO \ degradation \tag{12}$$

$$O_2^{\cdot-} + Dye \rightarrow MO \ degradation. \tag{13}$$
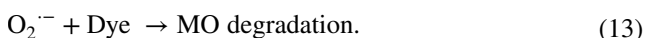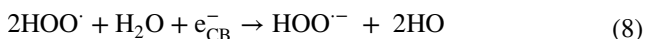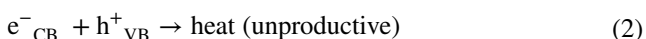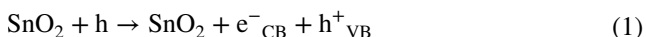
4 Conclusions

In summary, the SnO_2 NPs were biosynthesized by using aqueous leaf extract of C. G. This route is the green, rapid, eco-friendly and non-toxic for the synthesis of SnO_2 NPs using easily available C. G., which acts as reducing and stabilizing agent. The phytochemical screening confirmed that the presence of rich amount of metabolites like saponins, phenols, alkaloids, terpenoids, flavonoids, proteins and quinons are found in leaf extract. The size, structure and morphology of biosynthesized SnO_2 NPs were examined by XRD, FE-SEM, HR-TEM, DRS and EDS analysis. The XRD indicates the tetragonal structure of SnO_2 NPs. FE-SEM shows spherical morphology with slight agglomeration. The average crystallite size of SnO_2 NPs were found to be in the range 30–40 nm which is confirmed by XRD and TEM analysis. The FT-IR analysis of aqueous leaf extract confirmed the presence of hydroxyl group, aldehydes, amines and aromatic rings which are responsible for biochemical transformation. The DRS spectrum confirmed the biosynthesized SnO_2 NPs has high absorption with 3.1 eV band gap. The photocatalyst SnO_2 degrades the MO (20 ppm) dye upto 80%, within 210 min.

References

1. J.F.S. Fernando, M.P. Shortell, C.J. Noble, J.R. Harmer, E.A. Jaatinen, E.R. Waclawik, ACS Appl. Mater. Interfaces **8**, 14271 (2016)
2. G.K. Prashanth, P.A. Prashanth, U. Bora, M. Gadewar, B.M. Nagabhushana, S. Ananda, G.M. Krishnaiah, H.M. Sathyananda, Karbala Int. J. Mod. Sci. **1**, 67 (2015)
3. S. Raut, P.V. Thorat, R. Thakre, Int. J. Sci. Res. **4**, 1225 (2015)
4. S.M.H. Mashkani, A.S. Nasab, J. Mater. Sci. Mater. Electron. **28**, 4345 (2017)
5. M. Salavati-Niasari, F. Soofivand, A. Sobhani-Nasab, M. Shakouri-Arani, M. Hamadanian, S. Bagheri, J. Mater. Sci. Mater. Electron. **28**, 14965 (2017)
6. S.S.H. Mashkani, A. Nasab, J. Mater. Sci. Mater. Electron. **28**, 16459 (2017)
7. A.N. Naje, A.S. Norry, A.M. Suhail, IJIRSET 2, 7068 (2013)
8. L.I. Nadaf, K.S. Venkatesh, IOSR J. Appl. Chem. **9**, 01 (2016)
9. M.B. Suwarnkar, A.N. Kadam, G.V. Khade, N.L. Gavade, K.M. Garadkar, J. Mater. Sci. Mater. Electron. **27**, 843 (2016)
10. J.H. Lee, S.J. Park, J. Am. Ceram. Soc. **76**, 777 (1993)
11. S. Blessi, M.M.L. Sonia, S. Vijayalakshmi, S. Pauline, Int. J. Chem. Technol. Res. **6**, 2153 (2014)
12. Y. Liu, E. Koep, M. Liu, Chem. Mater. **17**, 3997 (2005)
13. M. Azizi, S.S. Abbas, W.R.W. Baharom, Mater. Lett. **91**, 31 (2013)
14. K.N. Thakkar, S.S. Mhatre, R.Y. Parikh, Nanomedicine **6**, 257 (2010)
15. S. Panigrahi, S. Kundu, S.K. Ghosh, S. Nath, T. Pal, J. Nanopart. Res. **6**, 411 (2004)
16. K.B. Narayanan, N. Sakthivel, Adv. Colloid Interface Sci. **156**, 1 (2010)
17. J.K. Sharma, M.S. Akhtar, S. Ameen, P. Srivastava, G. Singh, J. Alloys Compd. **632**, 321 (2015)
18. R.M. Thangavelu, D. Gunasekaran, M.I. Jesse, S.U.M. Riyaz, D. Sundarajan, K. Krishnan, Arab. J. Chem. **11**, 48 (2018)
19. B. Vaseeharan, C.G. Sargunar, Y.C. Lin, J.C. Chen, Nanotechnol. Dev. **2**, 2 (2012)
20. V.V. Gawade, N.L. Gavade, H.M. Shinde, S.B. Babar, A.N. Kadam, K.M. Garadkar, J Mater. Sci. Mater. Electron. **28**, 14033 (2017)
21. V. Kumar, S. Yadav, J. Chem. Technol. Biotechnol. **84**, 151 (2009)
22. C. Vidya, S. Hiremath, M.N. Chandraprabha, M.A.L. Antonyraj, I.V. Gopal, A. Jain, K. Bansal, Int. J. Curr. Eng. Technol. **1**, 118 (2013)
23. N. Srivastava, M. Mukhopadhyay, Ind. Eng. Chem. Res. **53**, 13971 (2014)
24. P.S. Kumar, E. Suresh, S. Kalavathy, Sch. Acad. J. Pharm. **2**, 135 (2013)
25. V.N. Verma, ILCPA **20**, 74 (2014)

26. R. Dhivya, K. Manimegalai, J. Pharmacogn. Phytochem. **2**, 28 (2013)
27. J. Mayandi, M. Marikkannan, V. Ragavendran, P. Jayabal, J. Nanosci. Nanotechnol. **2**, 707 (2014)
28. K. Elumalai, S. Velmurugan, S. Ravi, S. Kathiravan, S. Ashok kumar, Spectrochim. Acta. Biomol. Spectrosc. **143**, 158 (2015)
29. A. Khusro, C. Aarti, J.P. Preetamraj, S.G. Panicker, Int. J. Pharm. Pharm. Sci. **6**, 874 (2014)
30. S. Tazikeh, A. Akbari, A. Talebi, E. Talebi, Mater. Sci. Pol. **32**, 98 (2014)
31. M.M. Kumari, D. Philip, Powder Technol. **270**,, 312 (2015)
32. A. Khusro, C. Aarti, J.P. Preetamraj, S.G. Panicker, Int. J. Pharm. **6**, 874 (2014)
33. S.K. Kansal, M. Singh, D. Sud, J. Hazard. Mater. **141**, 581 (2006)
34. D.P. Kumar, N.L. Reddy, M. Karthikeyan, N. Chinnaiah, V. Bramhaiah, V.D. Kumari, M.V. Shankar, J. Colloid Interface. **477**, 201 (2016)
35. S. Abbasi, M. Hasanpour, J. Mater. Sci. Mater. Electron. **28**, 1307 (2017)
36. H. Yuan, X.U. Jiaqiang, Int. J. Chem. Eng. Appl. **1**, 241 (2010)